

Crystal structures and superconducting properties of metallic double-chain based cuprate $\text{Pr}_2\text{Ba}_4\text{Cu}_7\text{O}_{15-\delta}$

Masahide Hagawa¹, Michiaki Matsukawa¹, Kota Niinuma¹, Reiya Kudo¹, Yuto Mizusihima¹, Naohisa Kawarada¹, Hajime Yamamoto², Kazuhiro Sano³, Yoshiaki Ōno⁴ and Takahiko Sasaki⁵

¹Faculty of Science and Engineering, Iwate University, Morioka 020-8551, Japan

²Institute of Multidisciplinary Research for Advanced Materials, Tohoku University, Sendai 980-8577, Japan

³Department of Physics Engineering, Mie University, Tsu 514-8507, Japan

⁴Department of Physics, Niigata University, Niigata 950-2181, Japan

⁵Institute for Materials Research, Tohoku University, Sendai 980-8577, Japan

(Dated: February 20, 2024)

We demonstrated the lattice structures and the superconducting phases of metallic double-chain based cuprate $\text{Pr}_2\text{Ba}_4\text{Cu}_7\text{O}_{15-\delta}$ exhibiting higher T_c . After the oxygen heat treatment on citrate pyrolysis precursors, their reduction treatment followed by a quench procedure caused higher T_c samples with 26.5~30 K. The crystal structural parameters for the superconducting sample ($\delta = 0.81$) were analyzed from the powder synchrotron X-ray diffraction data using RIETAN-FP program. The effect of magnetic field on the superconducting phase of these samples with different oxygen defects ($\delta = 0.73, 0.81$ and 0.87) was examined, for our understanding of the superconducting magnetic field-temperature phase diagram. For the $\delta = 0.87$ sample with $T_c \sim 30$ K, the resistive critical field H_{c^*} was estimated to be 13 T at 4.2 K. The oxygen deficiency dependence on $T_{c,on}$ for our samples was compared with the data of several other groups.

INTRODUCTION

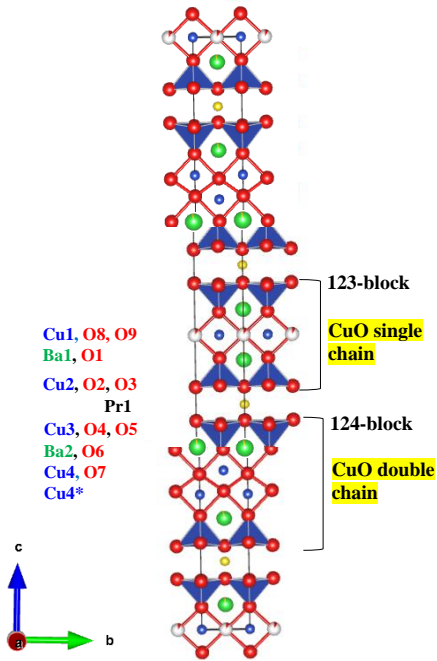


FIG. 1. Projection along (100) of the crystal structure of $\text{Pr}_2\text{Ba}_4\text{Cu}_7\text{O}_{15-\delta}$. The CuO single-chain 123- and double-chain 124-blocks are alternatively stacked along the c -axis. The nomenclature of atomic positions is displayed on the left hand side. The polyhedral planar part represents CuO_2 plane site.

Since the discovery of superconductivity in the metallic double-chain based cuprate $\text{Pr}_2\text{Ba}_4\text{Cu}_7\text{O}_{15-\delta}$ (Pr247)[1], experimental and theoretical studies on this system have been

extensively reported [2–8]. The Pr247 system is considered to be an intermediate compound between the 2D high- T_c layered cuprate superconductors and the quasi-1D organic superconductors, as well as the spin-ladder compounds. It is well known that the spin ladder system exhibits superconductivity with $T_c \sim 12$ K only under an external pressure above ~ 3.0 GPa [9]. $\text{Pr}_2\text{Ba}_4\text{Cu}_7\text{O}_{15-\delta}$ cuprate is an electron-doped superconductor with $T_c \sim 15$ K at ambient pressure through controlling the amount of oxygen deficiency due to a reduction treatment.

For the crystal structure of $\text{Pr}_2\text{Ba}_4\text{Cu}_7\text{O}_{15-\delta}$ (Fig.1), the $\text{PrBa}_2\text{Cu}_3\text{O}_{7-\delta}$ (Pr123)-type blocks containing the CuO single chains are alternatively stacked along the c -axis with the $\text{PrBa}_4\text{Cu}_7\text{O}_{15-\delta}$ (Pr124)-type ones containing the CuO double chains. The Pr123 and Pr124 compounds show no superconductivity associated with the CuO_2 planes because the strong hybridization between Pr-4f and O-2p orbitals suppresses their metallic conduction [10]. Furthermore, an angle-resolved photoemission study revealed the CuO single chain in Pr123 and the CuO double chain in Pr124 exhibit insulating and metallic characters, respectively, although both chains are approximately quarter filling [11]. Recently, a Cu nuclear quadrupole resonance study on Pr247 with a full volume fraction of superconductive phase has revealed that the CuO_2 plane is an antiferromagnetically insulating state at 2 K despite its bulk superconductivity[12, 13]. This finding strongly indicates that the superconductivity in Pr247 appears along the metallic CuO double chains, considering the oxygen deficiency at the CuO single chain site. For our further understanding of dimensionality in the electronic state of CuO double chains, the lattice, transport, and magnetic properties of Pr247 have been examined under an external pressure. Both the resistivity and magnetization measurements revealed that the superconducting behaviors in Pr247 are suppressed by the pressure effect[14, 15]. The negative pressure dependences

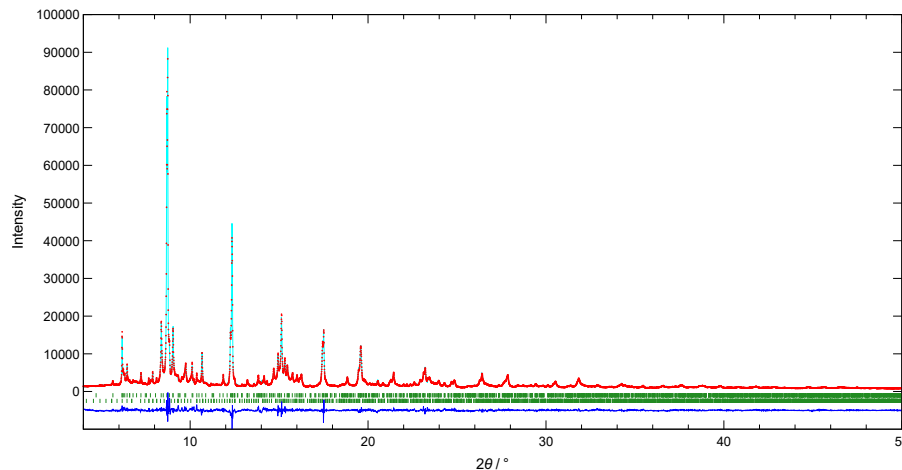


FIG. 2. Powder synchrotron X-ray diffraction pattern on the superconducting sample $\text{Pr}_2\text{Ba}_4\text{Cu}_7\text{O}_{15-\delta}$ ($\delta = 0.81$) at room temperature. The calculated and residual curves are also shown using RIETAN-FP program for two-phase Rietveld refinement. The upper and lower tick marks represent peak positions for the $\text{Pr}_2\text{Ba}_4\text{Cu}_7\text{O}_{15-\delta}$ and BaCuO_2 phases, respectively. The mass fractions of Pr247 and BaCuO_2 were estimated to be 96.0% : 4.0%. $\lambda = 0.42 \text{ \AA}$.

of the superconducting phase are qualitatively explained by the normal to superconductive phase diagram of CuO double chains on the basis of Tomonaga-Luttinger liquid theory[6]. The magneto resistance (MR) effect of the normal phase of Pr247 is enhanced due to applied pressure, which is probably related to a warped Fermi surface induced by the pressure. Taniguchi et al, found out from in-situ XRD experiments under pressure that the a -axis lattice parameter across the CuO double chain along the b -axis is elongated against pressure above 2.0 GPa[16].

In this paper, we demonstrate crystal structures and superconducting properties of metallic double-chain based cuprate $\text{Pr}_2\text{Ba}_4\text{Cu}_7\text{O}_{15-\delta}$. In the next section, the experimental outline is described. In Section 3, we present the powder synchrotron X-ray diffraction data on the superconducting sample $\text{Pr}_2\text{Ba}_4\text{Cu}_7\text{O}_{15-\delta}$ ($\delta = 0.81$) using RIETAN-FP program for two-phase $\text{Pr}_2\text{Ba}_4\text{Cu}_7\text{O}_{15-\delta}$ and BaCuO_2 . We examine the magnetic field effect on the superconducting phase of these three samples with different oxygen defects ($\delta = 0.73, 0.81$ and 0.87). The superconducting magnetic field-temperature phase diagram is determined from the low-temperature MR effect. Concluding remarks are given in the final section.

EXPERIMENT

Precursors for the superconducting cuprates $\text{Pr}_2\text{Ba}_4\text{Cu}_7\text{O}_{15-\delta}$ were prepared through spontaneous combustion reactions using a citrate pyrolysis method[3, 17]. (refer to a video file recording the typical self-ignition process attached in Appendix A in ref.[18]). The fine powders crushed from their precursors were pressed to form a disk pellet and its pellet was cut into several pieces. These smaller pieces from the original pellet were initially set in a cage of Ag

fine meshes and were then annealed under ambient oxygen atmosphere at 890-891 °C for 96-110 hours in an electric tube furnace. A narrow stability range of annealing temperature between 890 and 891 °C allowed synthesis of pure phase of Pr247 with the aid of a three-zone temperature controller. As for the as-sintered samples, oxygen removed procedures are further needed in order to realize their superconducting phases. The oxygen contents were reduced through heat treatment in a vacuum atmosphere at 500-600 °C for 3-5 days. We conducted gravimetric analysis on the present three samples and their oxygen defects were estimated to be $\delta = 0.73, 0.81$, and 0.87 (referred as samples #2-1, #3, and #4). An electron probe micro analysis on the as-sintered samples prepared under a similar oxygen annealing condition showed the average oxygen content = ~ 14.96 . A quench process in air from 300 °C down to room temperature was an effective approach to achieve better superconducting properties, in comparison to furnace cooling procedures in our previous synthesis. For the $\delta = 0.73, 0.81$, and 0.87 oxygen-reduction samples, the dimension of their rectangular shape and their relative density (d) are given in Table I. We carried out powder synchrotron X-ray diffraction measurements on the fine powders crashed from the superconducting bulk samples at SPring-8 beamline BL02B2 at room temperature. The wavelength of the incident X-ray, $\lambda = 0.42 \text{ \AA}$, was utilized. The collected diffraction patterns were fitted using RIETAN-FP program two-phase Rietveld refinement[19]. The electric resistivity measurement was measured by the dc four-terminal method. The magneto-transport up to 9 T was measured by the ac four-probe method using a physical property measuring system (PPMS, Quantum Design), from 4 K to 40 K at several magnetic fields ($\mu_0 H = 0, 1, 3, 6$, and 9 T) after the zero-field-cooling (ZFC) scan. The low-temperature magneto-resistance (MR) effect (up to 14 T) was measured

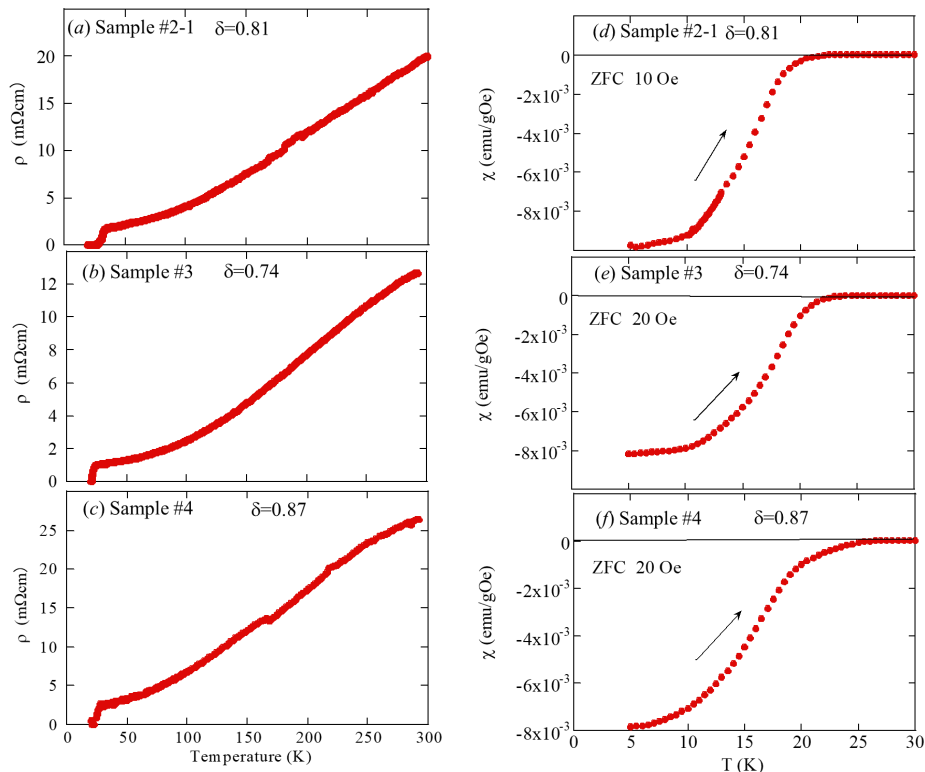


FIG. 3. Temperature dependences of electric resistivities for the superconducting $\text{Pr}_2\text{Ba}_4\text{Cu}_7\text{O}_{15-\delta}$. (a) sample #2-1 with $\delta=0.81$, (b) sample #3 with $\delta=0.74$, and (c) sample #4 with $\delta=0.87$. In the inset, the low-temperature magnetization curves measured under a zero field cooling (ZFC) scan are plotted, to clarify a bulk superconductivity.

in a superconducting magnet (15T-SM) at Institute for Materials Research, Tohoku University. The electric current I was applied longitudinally to the sample; consequently, the applied magnetic field H was transverse to the sample (because $H \perp I$). The dc magnetization was performed under ZFC in a commercial superconducting quantum interference device magnetometer (Quantum Design, MPMS).

RESULTS AND DISCUSSION

Figure 1 shows the schematic projection along (100) of the crystal structure of $\text{Pr}_2\text{Ba}_4\text{Cu}_7\text{O}_{15-\delta}$. The CuO single-chain and double-chain blocks are alternatively stacked along the c -axis. The two-phase Rietveld refinement results for the as-sintered and oxygen-reduction samples of $\text{Pr}_2\text{Ba}_4\text{Cu}_7\text{O}_{15-\delta}$ ($\delta=0, 0.73$, and 0.81) are listed in Table I. The typical powder synchrotron X-ray diffraction data on the superconducting sample $\text{Pr}_2\text{Ba}_4\text{Cu}_7\text{O}_{15-\delta}$ ($\delta=0.81$) at room temperature are given in Fig. 2. The calculated and residual curves are also plotted using RIETAN-FP program for two-phase $\text{Pr}_2\text{Ba}_4\text{Cu}_7\text{O}_{15-\delta}$ and BaCuO_2 . The mass fractions of $\text{Pr}247$ and BaCuO_2 were estimated to be 96.0% : 4.0%.

Here, we give some comments on the atomic position parameters of $\text{Pr}_{2.2}\text{Ba}_{3.8}\text{Cu}_7\text{O}_{15-\delta}$ ($\delta=0.8$) listed in Table II [20].

In the present Rietveld refinement, we assume that the Ba1 and Ba2 sites are partially replaced by Pr ions with same occupancy rates of 0.05 in the 123 and 124 blocks, respectively. For the Pr123 compound, it has been reported that the Pr rich and Ba poor compositions $\text{Pr}_{1+x}\text{Ba}_{2-x}\text{Cu}_3\text{O}_{7-\delta}$ are stable against the stoichiometric one from the single phase diagram studies [23]. These findings strongly suggest that to form the Pr123 single phase, the Ba sites must have partial Pr ions. This tendency is naturally extended to the Pr124 and Pr247 systems. The occupancy rates at the oxygen sites O8 and O9 in the 123 block are set to be 0.1, to match the oxygen defect.

A vacuum reduction treatment of the as-sintered samples introduces oxygen defects, resulting in carrier doping effect associated with the appearance of superconducting phases. It is well known that higher T_c samples are closely related to larger oxygen defects accompanied by the c -axis elongation of Pr247. The variations of the lattice parameters due to oxygen removal are almost similar to the previous ones[2]. In Table III, the selected bond lengths for $\text{Pr}_2\text{Ba}_4\text{Cu}_7\text{O}_{15-\delta}$ determined by the powder synchrotron X-ray diffraction patterns are listed. Comparing the interatomic distances for the superconducting and non-superconducting samples, we detected no clear differences in all the bond lengths between both the samples. As for the $\text{Cu}_{\text{ch}}\text{-O}_{\text{ch}}(\text{Cu4-O7} \parallel c)$ bond length cor-

TABLE I. Lattice parameters and superconducting properties for the as-sintered and oxygen-reduction samples of $\text{Pr}_2\text{Ba}_4\text{Cu}_7\text{O}_{15-\delta}$ ($\delta = 0, 0.73, 0.81, \text{ and } 0.87$). In details, see the corresponding text and references. f_{SC} : the superconducting volume fraction estimated from the ZFC magnetization data at low temperatures. $T_{\text{c,on}}$: defined as the onset temperature of resistive drop. The reliability factors for four samples are listed. For the oxygen defect samples with $\delta = 0.73, 0.81, \text{ and } 0.87$, the dimension of their rectangular shape and their relative density (d) are also given.

Sample No.	oxygen defect δ	a (Å)	b (Å)	c (Å)	f_{SC} (%)	$T_{\text{c,on}}$ (K)	R_{wp} (%)	R_{p} (%)	R_{B} (%)
#1	-	3.87958 (5)	3.89975 (1)	50.6281(2)	-	-	7.95	5.61	1.54
#2-0	-	3.8791(5)*	3.8997(5) *	50.628(6)*	-	-	11.9*	9.14*	4.24*
#2-1	0.81 $1.1 \times 3.7\text{mm}^2$	3.88287(4) 4.2 mm	3.89003(4) $d = 89\%$	50.8485(4)	63	28.0	6.62	4.86	2.83
#3	0.73 $0.8 \times 4.1\text{mm}^2$	3.8821(1) 5.7 mm	3.8899(1) $d = 96\%$	50.8160(6)	59	26.5	4.88	3.69	4.36
#4	0.87 $2.1 \times 5.0\text{mm}^2$	- 5.5 mm	- $d = 84\%$	-	53	30.0	-	-	-
ref. [2]	-	3.89127(9)	3.90714(8)	50.695(1)	-	-	4.51	3.31	-

*Ultima IV Cu-K α

TABLE II. Atomic position parameters of $\text{Pr}_{2.2}\text{Ba}_{3.8}\text{Cu}_7\text{O}_{15-\delta}$ ($\delta=0.8$). In our Rietveld refinement of the synchrotron and conventional X-ray diffraction patterns for all the samples investigated, similar atomic position parameters are adopted. B is an isotropic thermal parameter. For oxygen atoms, B is fixed to be 1.0 \AA^2 .

#2-1	$\delta=0.81$	(Ammm)					
Atom	Site	Occ.	x	y	z	$B (\text{\AA}^2)$	
Pr1	4j	1.0	0.5	0.5	0.11559(4)	0.15(2)	
Ba1	4j	0.95	0.5	0.04188(3)	0.5	0.51(2)	
Pr2	4j	0.05	0.5	0.04188(3)	0.5	0.15(2)	
Ba2	4j	0.95	0.5	0.18865(3)	0.5	0.51(2)	
Pr3	4j	0.05	0.5	0.18865(3)	0.5	0.15(2)	
Cu1	2a	1.0	0.0	0.0	0.0	0.33(2)	
Cu2	4i	1.0	0.0	0.0	0.08073(7)	0.33(2)	
Cu3	4i	1.0	0.0	0.5	0.15027(7)	0.33(2)	
Cu4	4i	1.0	0.0	0.0	0.22965(6)	0.33(2)	
O1	4i	1.0	0.0	0.0	0.0386(4)	1.0	
O2	4j	1.0	0.5	0.0	0.0828(4)	1.0	
O3	4i	1.0	0.0	0.5	0.0861(3)	1.0	
O4	4j	1.0	0.5	0.0	0.1486(4)	1.0	
O5	4i	1.0	0.0	0.5	0.1421(3)	1.0	
O6	4i	1.0	0.0	0.0	0.1935(3)	1.0	
O7	4i	1.0	0.0	0.5	0.2355(3)	1.0	
O8	2b	0.1	0.0	0.5	0.0	1.0	
O9	2d	0.1	0.5	0.0	0.0	1.0	

responding to the inter-chain distance along the c -axis in the 124 block, it seems to be slightly shorter in the $\delta = 0.81$ sample with $T_{\text{c,on}}=28$ K than that in the non-superconducting as-sintered sample. The normal to superconducting phase diagram of a CuO double-chain has been investigated on the basis of Tomonaga-Luttinger liquid theory[6]. In the $n - t_{pp}$ binary phase diagram, n is electron density in the d band of the CuO double chain and t_{pp} is hopping energy between near-

est neighbor oxygen sites occupied by $2p_{\sigma}$ orbitals. While the system initially remains in the normal phase, the electron carrier doping effect causes a phase transition of it from the normal to superconducting state. Furthermore, a shrinkage of the distance between two chains of a CuO double chain gives rise to an increase in the hopping energy t_{pp} . As a result of the heavy oxygen defects, it is expected that the double-chain system in the normal phase is varied diagonally towards the

TABLE III. Selected bond lengths for $\text{Pr}_2\text{Ba}_4\text{Cu}_7\text{O}_{15-\delta}$, determined by the powder synchrotron X-ray diffraction patterns. See Fig. 1 for positional notation of Pr247. The atomic positions for Pr 124 and Pr123 are referred to the published data[21, 22]. Cu_{pl} and Cu_{ch} denote the planar and chain copper sites, respectively. O_{ap} and O_{ch} are the apical and double-chain oxygen sites.

bond length (Å)	Pr247/ $\delta=0.81$		Pr247 ref. [2]		Pr124	Pr123
	124-block	#2-1 123-block	124-block	123-block	ref. [21]	ref. [22]
$\text{Cu}_{\text{pl}}\text{-Cu}_{\text{pl}}$	Cu2-Cu3 3.528(5)		Cu2-Cu3 3.525		Cu2-Cu2 3.508	Cu2-Cu2 3.554
$\text{Cu}_{\text{pl}}\text{-O}_{\text{ap}}$	Cu3-O6 2.183(4)	Cu2-O1 2.095(20)	Cu3-O6 2.196	Cu2-O1 2.136	Cu2-O1 2.234	Cu2-O2 2.232
$\text{Cu}_{\text{ch}}\text{-O}_{\text{ap}}$	Cu4-O6 1.835(3)	Cu1-O1 2.010(20)	Cu4-O6 1.884	Cu1-O1 1.957	Cu1-O1 1.836	Cu1-O2 1.854
$\text{Cu}_{\text{ch}}\text{-O}_{\text{ch}}(\parallel c)$	Cu4-O7 1.735(16)	-	Cu4-O7 1.807	-	Cu1-O4 1.876	-
$\text{Cu}_{\text{ch}}\text{-O}_{\text{ch}}(\parallel b)$	Cu4-O7 1.975(3)	-	Cu4-O7 1.960	-	Cu1-O4 1.955	-

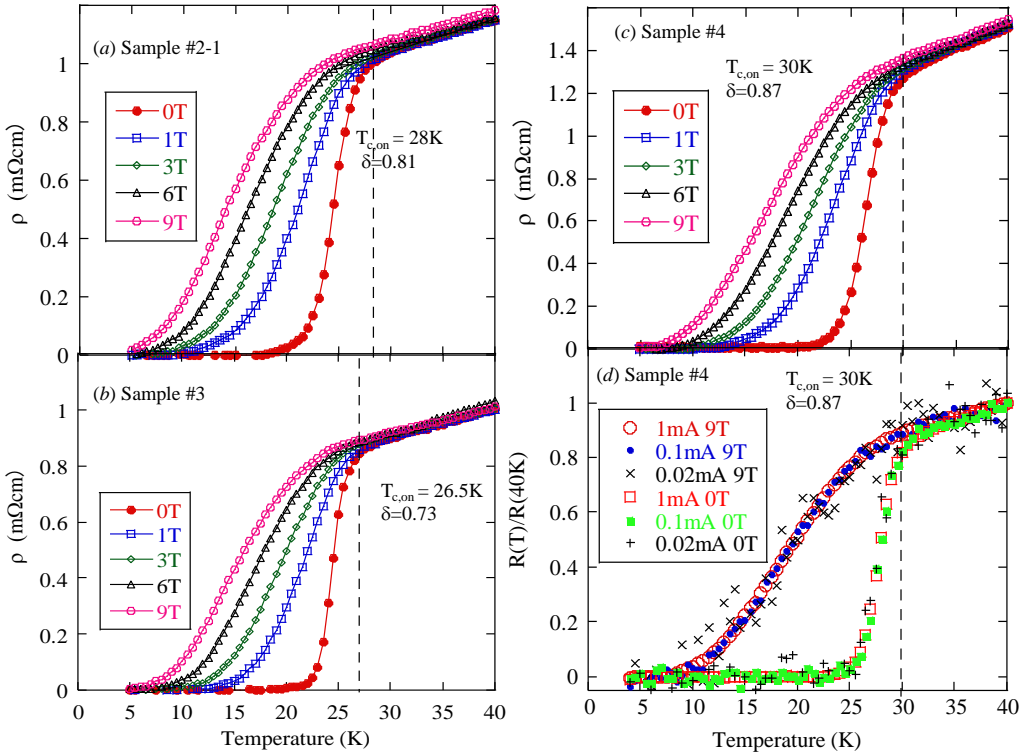


FIG. 4. Low temperature dependences of electric resistivities for the superconducting $\text{Pr}_2\text{Ba}_4\text{Cu}_7\text{O}_{15-\delta}$ measured at the several applied fields ($\mu_0H=0, 1, 3, 6,$ and 9 T). (a) sample #2-1 with $\delta=0.81$, (b) sample #3 with $\delta=0.74$, and (c) sample #4 with $\delta=0.8$. In (d), the data for the sample #4 are taken at 0T and 9T for the applied current $I=1, 0.1$ and 0.02 mA. Broken lines are guides for the eyes.

superconducting phase on the $n - t_{pp}$ plane, realizing double-chain driven superconductivity.

Next, in Fig. 3, we show the temperature dependences of electric resistivities for the superconducting $\text{Pr}_2\text{Ba}_4\text{Cu}_7\text{O}_{15-\delta}$. The low-temperature magnetization curves measured under a zero field cooling (ZFC) scan are also plotted, to clarify a bulk superconductivity. In addition, we examined the mag-

netic field effect on the superconducting phase of these three samples with different oxygen defects, as shown in Figures 4, 5 and 6(a). First of all, the reduction heat treatment increased the onset temperature of superconductive transition $T_{\text{c,on}}$ from 26.5 K at $\delta=0.7$, through 28.0 K at $\delta=0.81$ one, up to 30.0 K at $\delta=0.87$. From our magnetization data for the three samples, their superconducting volume fractions f_{SC} reached over 50

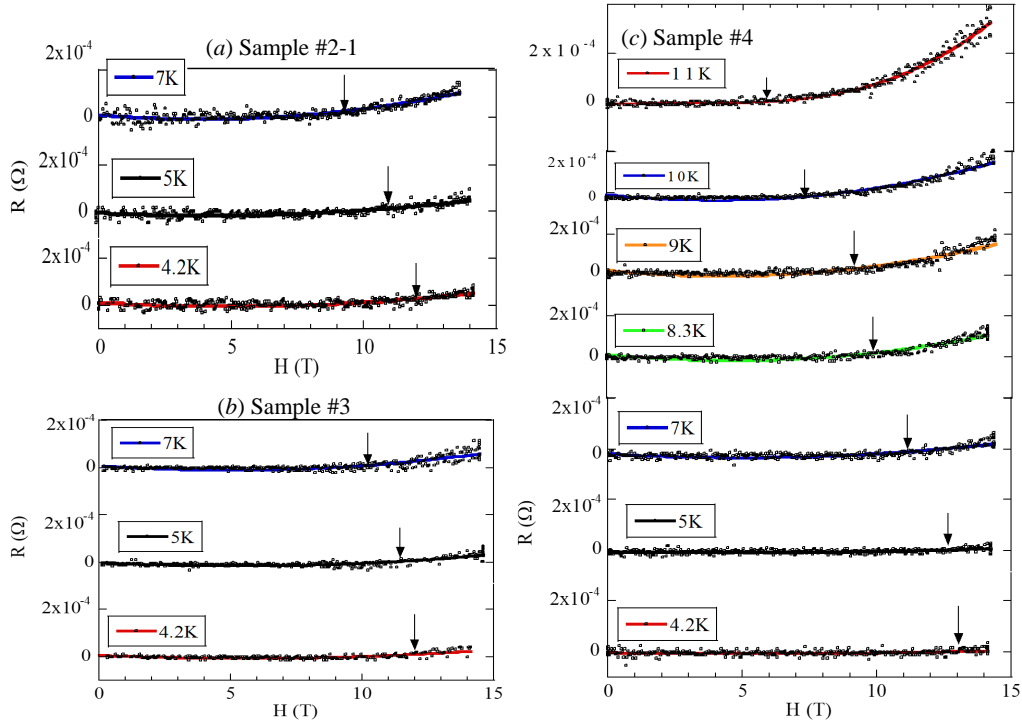


FIG. 5. Low-temperature magneto-resistance effect as a function of magnetic field up to 14 T for the superconducting $\text{Pr}_2\text{Ba}_4\text{Cu}_7\text{O}_{15-\delta}$. (a) sample #2-1 and (b) sample #3 at $T = 4.2$ K, 5 K, and 7 K. (c) sample #4 at $T = 4.2$ K \sim 11 K. The arrow symbols denote the critical fields H_c^* , where a zero-resistance state is violated at selected temperatures upon increasing applied field. Lines are guides for the eyes.

%. Furthermore, a zero-resistance state of these samples was observed below $T_{c,\text{zero}} = 20 \sim 22$ K at 0 T. On the other hand, the room-temperature resistivity was enhanced from ~ 12 m Ω cm to ~ 26 m Ω with increasing the oxygen defect. This behavior is probably related to the highly insulating state of the CuO_2 planes due to the removal of single-chain site oxygen in 123 block, as suggested in the oxygen content study on the Pr123 compound [22]. In the $\text{PrBa}_2\text{Cu}_3\text{O}_{7-\delta}$ system, it was reported that the room-temperature resistivity is increased by about three orders of magnitude from $\delta = 0$ to $\delta \sim 0.5$. The present Pr247 reduced samples showed the higher residual resistance ratios (RRR), $\rho(\text{RT})/\rho(30\text{K})$, ranging from 10 to 12, as pointed out in our previous study [24]. Assuming that a model of parallel resistors along the b axis consists of CuO chain and CuO_2 plane resistances, it is reasonable to consider the contribution of a doped double chain alone to $\rho(T)$, because of ignoring electric conducting path in a highly insulating plane.

The application of external magnetic field up to 9 T caused widely broadening of the resistive transition curves accompanied by disappearance of a zero resistance state. $T_{c,\text{on}}$ seems to be stable with respect to the applied field, in spite of a rapid degradation of $T_{c,\text{zero}}$.

We examined the resistive transition profiles under 9 T as

a function of the electric current ranging from 0.02 mA to 1 mA. In our present experiment (Fig. 4 (d)) [25], there were no significant differences in the resistive drops among 0.02, 0.1 and 1 mA. It is not made clear that the motion of magnetic flux due to Lorentz force affects these broadening behaviors, because of the applied current densities limited to lower values of ~ 10 to 40 mA/cm 2 . Our results are reminded of the magnetic field effect on the superconducting phases in the hole doped two-leg ladder compound $\text{Sr}_2\text{Ca}_{12}\text{Cu}_{24}\text{O}_4$ and high- T_c cuprate $(\text{La}_{1-x}\text{Sr}_x)_2\text{CuO}_4$ [26, 27].

From the low-temperature electric resistivity data for the superconducting sample #4 under several applied fields ($\mu_0 H = 0, 1, 3, 6,$ and 9 T), we obtained the onset critical temperature as a function of magnetic field $T_{c,\text{on}}(H)$. Using the Werthamer-Helfand-Hohenberg (WHH) formula in the dirty limit, $\mu_0 H_{c2}(0) = -0.69 T_c (dH_{c2}(T)/dT)|_{T=T_c}$ [28], the upper critical field at $T = 0$ K, $H_{c2}(0)$ was evaluated to be ~ 45 T. According to $H_{c2} = \phi_0 / 2\pi \xi^2$, we obtained the Ginsburg-Landau coherence length $\xi \sim 27$ Å, which is comparable to the in-plane coherence length for $(\text{La}_{1-x}\text{Sr}_x)_2\text{CuO}_4$ single-crystal thin films [29]. To further establish the superconducting high-field phase diagram, we determined from the low-temperature MR effect the resistive critical field as a function of temperature $H_c^*(T)$, where a zero-resistance state

is violated at selected temperatures upon increasing applied field. For the present samples, H_c^* is estimated to be 12-13 T at 4.2 K. In the resistive crossover region from $T_{c,on}(H)$ to $H_c^*(T)$ line, it is hard to distinguish between dissipation due to a melting of vortex lattice and an intrinsic effect associated with the double-chain induced superconductivity. The higher critical fields are probably attributed to the improved sample preparation process using the three-zone electric furnace, compared with the lower H_c^* value (~ 4 T at 4 K) for the previous samples with higher $T_{c,on} = 26.5$ K [15]. Additionally, the quenched treatment just after vacuum reduction annealing contributes to the enhanced superconducting properties for the present samples. These procedures are related to further improvements of weak links between the superconducting grains.

Finally, in Fig. 6 (c), we summarize $T_{c,on}$ vs oxygen deficiency for our samples, compared with the data of several other groups [12, 14, 30]. It is noted that the higher T_c samples around ~ 26 K are synthesized by using the citrate pyrolysis based precursors under the different heat treatment conditions. On the other hand, the lower T_c samples are annealed under ambient and high pressure oxygen atmospheres by using a solid-state reaction method for mixed fine powders. It is true that the value of T_c is closely dependent on the oxygen defects. However, the differences between two-types of the lower and higher T_c samples are difficult to explain on the basis of the oxygen occupancy at the CuO single chain sites only. According to high-resolution electron microscopy studies [25, 30] on Pr247, there exist stacking faults in the -123-124-123-124- (-S-D-S-D-) regular sequence along the c axis as shown in Fig.1. Here, S and D correspond to the single and double CuO chain blocks. For instances, the stacking faults such as the -123-123-123-124- (-S-S-S-D-) irregular sequence are reported for the citrate pyrolysis samples. For the Y247 system [31, 32], it is also concluded that the difference in T_c values is not attributed to the oxygen occupancy but micro structures. Through TEM measurements on different samples with two-types of preparation methods, stacking faults along the c -axis are observed more frequently in a polymerized-complex sample with $T_c = 93$ K than in a solid-state reaction sample with $T_c = 65$ K. Accordingly, we expect that higher T_c samples driven by CuO double chain superconductivity are related to stacking faults, although CuO₂ based layered superconductivity of Y247 is quite different from that of the present Pr247 system.

SUMMARY

We demonstrated the lattice structures and the superconducting phases of metallic double-chain based cuprate Pr₂Ba₄Cu₇O_{15- δ} exhibiting higher T_c . After the oxygen heat treatment on the citrate pyrolysis precursors in the three-zone temperature controlled furnace, their reduction treatment followed by a rapidly cooling procedure caused higher T_c samples with 28~30 K. We carried out the powder synchrotron

X-ray diffraction measurements on the as-sintered and vacuum reduction samples at Spring-8 beamline. In particular, the crystal structural parameters for the superconducting sample ($\delta = 0.81$) were investigated using RIETAN-FP program for two-phase Pr₂Ba₄Cu₇O_{15- δ} and BaCuO₂.

We examined the magnetic field effect on the superconducting phase of these three samples with different oxygen defects ($\delta = 0.73, 0.81$ and 0.87) and established the superconducting magnetic field-temperature phase diagram from the low-temperature MR effect. For the $\delta = 0.87$ sample with $T_c \sim 30$ K, H_c^* was estimated to be 13 T at 4.2 K. $H_{c2}(0)$ was evaluated to be ~ 45 T, resulting in the Ginsburg-Landau coherence length $\xi \sim 27$ Å. When oxygen deficiency dependence on $T_{c,on}$ for our samples was compared with the data of several other groups [12, 14, 30], better superconductive samples driven by CuO double chains have a close relationship with stacking faults along the c -axis.

The authors are grateful for M. Nakamura for his assistance in PPMS experiments at Center for Regional Collaboration in Research and Education, Iwate University. M. M thanks Prof. M. Hagiwara for his valuable comments. The synchrotron radiation experiments were performed at the BL02B2 of SPring-8.

-
- [1] M. Matsukawa, Y. Yamada, M. Chiba, H. Ogasawara, T. Shibata, A. Matsushita, and Y. Takano, *Physica C* 411 (2004) 101.
 - [2] Y. Yamada and A. Matsushita, *Physica C* 426-431 (2005) 213.
 - [3] M. Hagiwara, T. Shima, T. Sugano, K. Koyama, and M. Matsuura, *Physica C* 445-448 (2006) 111.
 - [4] Y. Wakisaka, K. Takubo, T. Sudayama, J. Y. Son, T. Mizokawa, M. Arita, H. Namatame, M. Taniguchi, S. Sekiya, K. Fukuda, F. Ishikawa, and Y. Yamada, *J. Phys. Soc. Jpn.* 77 (2008) 074710.
 - [5] J. Tada, M. Matsukawa, T. Konno, S. Kobayashi, M. Hagiwara, T. Miyazaki, K. Sano, Y. Ono, and A. Matsushita, *J. Phys. Soc. Jpn.* 82 (2013) 105003.
 - [6] K. Sano, Y. Ono, and Y. Yamada, *J. Phys. Soc. Jpn.* 74 (2005) 2885.
 - [7] T. Nakano, K. Kuroki, and S. Onari, *Phys. Rev. B* 76 (2007) 014515.
 - [8] K. Okunishi, *Phys. Rev. B* 75 (2007) 174514.
 - [9] M. Uehara, T. Nagata, J. Akimitsu, H. Takahashi, N. Mori, and K. Kinoshita, *J. Phys. Soc. Jpn.* 65 (1996) 2764.
 - [10] R. Fehrenbacher and T. M. Rice, *Phys. Rev. Lett.* 70 (1993) 3471.
 - [11] T. Mizokawa, C. Kim, Z.-X. Shen, A. Ino, T. Yoshida, A. Fujimori, M. Goto, H. Eisaki, S. Uchida, M. Tagami, K. Yoshida, A. I. Rykov, Y. Siohara, K. Tomimoto, S. Tajima, Y. Yamada, S. Horii, N. Yamada, Y. Yamada, and I. Hirabayashi, *Phys. Rev. Lett.* 85 (2000) 4779.
 - [12] S. Nishioka, S. Sasaki, S. Nakagawa, M. Yashima, H. Mukuda, M. Yogi and J. Shimoyama, *Appl. Phys. Express* 15 (2022) 023001.
 - [13] S. Watanabe, Y. Yamada, and S. Sasaki, *Physica C* 426-431 (2005) 473.
 - [14] F. Ishikawa, K. Fukuda, Y. Hiura, Y. Onda, A. Nakayama, Y. Yamada, A. Matsushita and T. Kagayama, *J. of Phys.: Conf. Ser.*

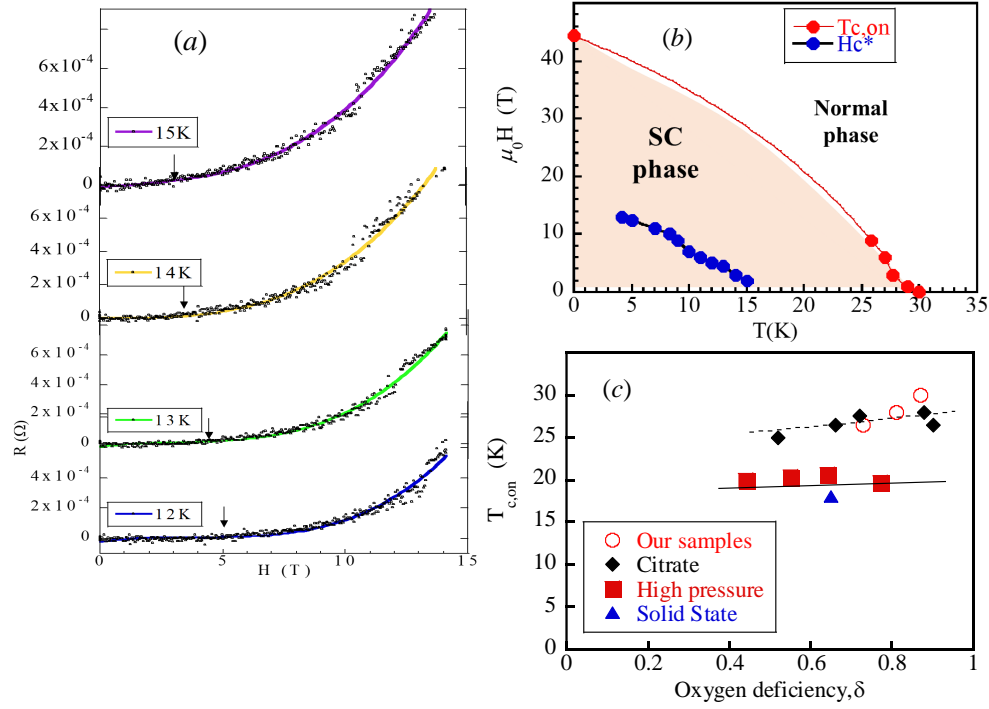


FIG. 6. (Color online) (a) Low-temperature magneto-resistance effect as a function of magnetic field up to 14 T for the superconducting $\text{Pr}_2\text{Ba}_4\text{Cu}_7\text{O}_{15-\delta}$ (sample #4) at $T=12\sim 15$ K. (b) Superconducting high-field phase diagram. $T_{c,on}(H)$ and $H_c^*(T)$ were taken from the temperature scan and magnetic field scan data. (c) $T_{c,on}$ vs oxygen deficiency for our samples (\circ). For comparison, \blacklozenge , \blacksquare , and \blacktriangle correspond to the data of Hagiwara et al.[30], Ishikawa et al.[14], and Nishioka et al.[12], respectively. Lines are guides for the eyes.

- 15 (2009) 052079.
- [15] M. Kuwabara, M. Matsukawa, K. Sugawara, H. Taniguchi, A. Matsushita, M. Hagiwara, K. Sano, Y. Ono, and T. Sasaki, *J. Phys. Soc. Jpn.* 85 (2016) 124704.
- [16] H. Taniguchi, Y. Nakarokkaku, R. Takahashi, M. Murakami, A. Nakayama, M. Matsukawa, S. Nakano, M. Hagiwara, and T. Sasaki, *J. Phys. Soc. Jpn.* 90 (2021) 015001.
- [17] T. Senzaki, M. Matsukawa, T. Yonai, H. Taniguchi, A. Matsushita, T. Sasaki and M. Hagiwara, *Functional Materials Synthesis and Physical Properties*, Recent Perspectives in Pyrolysis Research, chapter - DOI 10.5772/intechopen.95170 (18 pages) PUBLISHED 13 April 2022.
- [18] T. Teramura, M. Matsukawa, T. Senzaki, H. Taniguchi, K. Sano, Y. Ono, M. Hagiwara, *Physica B* 646 (2022) 414226.
- [19] F. Izumi and K. Momma, *Solid State Phenom.*, 130 (2007) 15-20.
- [20] P. Bordet, C. Chaillout, J. Chenavas, J. L. Hodeau, M. Marezio, J. Karpinski, and E. Kaldis, *Nature* 334 (1988) 596.
- [21] Y. Yamada, J. Ye, S. Horii, A. Matsushita, S. Kubo, *Journal of Physics and Chemistry of Solids* 62 (2001) 191.
- [22] M. E. Lopez-Morales, D. Rios-Jara, J. Taguena, R. Escudero, S. La Placa, A. Bezingue, V. Y. Lee, E. M. Engler, P. M. Grant, *Phys. Rev. B* 41 (1990) 6655.
- [23] B. Song, J.K. Liang, L.T. Yang, J.R. Chen, G.Y. Liu, H.F. Yang, G.H. Rao, *Appl. Phys. A* 77 (2003) 915.
- [24] K. Honnami, M. Matsukawa, T. Senzaki, T. Toyama, H. Taniguchi, K. Ui, T. Sasaki, K. Takahashi, M. Hagiwara, *Physica C* 585 (2021) 1353869.
- [25] T. Chiba, M. Matsukawa, J. Tada, S. Kobayashi, M. Hagiwara, T. Miyazaki, K. Sano, Y. Ono, T. Sasaki, and J. Echigoya, *J. Phys. Soc. Jpn.* 82 (2013) 074706.
- [26] T. Nakanishi, N. Motoyama, H. Mitamura, N. Takeshita, H. Takahashi, H. Eisaki, S. Uchida, and N. Mōri, *Phys. Rev. B* 72 (2005) 054520.
- [27] K. Kitazawa, S. Kambe, M. Naito, I. Tanaka and H. Kojima, *Jpn. J. Appl. Phys.* 28 (1989) L555.
- [28] N. R. Werthamer, E. Helfand, and P. C. Hohenberg, *Phys. Rev.* 147, (1966) 295.
- [29] M. Suzuki and M. Hikita, *Phys. Rev. B* 44, (1991) 249.
- [30] M. Hagiwara, S. Tanaka, T. Shima, K. Gotoh, S. Kanda, T. Saito, and K. Koyama, *Physica C* 468 (2008) 1217.
- [31] M. Kato, M. Nakanishi, T. Miyano, T. Shimizu, M. Kakihana, K. Yoshimura, K. Kosuge, *Journal of Solid State Chemistry* 139 (1998) 266-273.
- [32] Y. X. Guo, R. Hoier, T. Graf, and J. -Y. Genoud, *Phil. Mag.* B72 (1995) 383.